J. Cons. int. Explor. Mer, 35 (1): 78–86. June 1973.

Validity of ocean surface temperatures monitored from satellites

KARL-HEINZ SZEKIELDA[1]

Goddard Space Flight Center
Greenbelt, Maryland, U.S.A.

The ground truth (validity as established by ground data) of remote-sensed equivalent blackbody temperature (T_{BB}) as determined from Nimbus 2 satellite data was investigated over the Persian Gulf and the Somali Coast. The mean T_{BB} values recorded with the high resolution infrared radiometer (HRIR) were 0·1 C° cooler than the reported ship temperatures. The standard deviation for the difference between T_{BB} values and ship measurements was less than 1·3°C indicating that over cloud-free regions very good accuracy from orbiting sensors can be obtained.

Introduction

The Nimbus 2 satellite was launched on 15 May, 1966, in a near-circular orbit with an apogee height of 1180 km and a perigee height of 1095 km. Results obtained with this satellite were described, for instance, by Warnecke (1967), Pouquet (1968), La-Violette and Seim (1969), and Warnecke, Allison, McMillin and Szekielda (1971). In the following study, the observations with the HRIR (High Resolution Infrared Radiometer) were used for a comparison between remotely sensed ocean surface temperature and reported ship temperatures.

Background for the remote sensing of the ocean's sea surface temperature

The thermal behavior of a water surface can be regarded as that of a blackbody, and Planck's law is valid if the emissivity of water is considered to be :

$$W\lambda = (c_1\lambda^{-5})/[\exp(c_2/\lambda T) - 1]$$

where c_1 and c_2 are known as the first and second radiation constants, respectively, and have the values $c_1 = 3{\cdot}74 \times 10^{-12}$ W/cm^2 and $c_2 = 1{\cdot}44$ cm/°C.

The thermal radiation from the earth detected with an orbiting radiometer can therefore be used for a determination of temperature at the earth's surface if the emissivity of the area under investigation is known. This is valid only over cloud-free regions.

The radiative transfer equation over a cloud-free region in an atmospheric window can be written

$$N_W = N + \frac{1}{\pi}\int_{\lambda_1}^{\lambda_2} \Phi(\lambda)\, \varepsilon_S(\lambda)\, \beta\,(\lambda\tau_S) d\lambda,$$

where Φ is the filter function [$\Phi(\lambda) = 0$ outside the interval λ_1 λ_2], ε_S is the emissivity of the radiating surface, and $\beta(\lambda\tau_S)$ is the Planck function. The term N represents the energy absorbed by atmospheric gases and water vapour during the radiation from the earth's surface to satellite height. In this study, N is kept constant over the area under investigation; therefore, the reported temperatures should be regarded only as relative values, although the temperature changes in the same region are absolute.

The radiometer

A schematic representation of a scanning radiometer that can detect outgoing radiation from the earth aboard a satellite is given in Figure 1. The radiation emitted by the earth's surface reaches a scan mirror, which is inclined 45° to its own axis of rotation. This scanning rotates the field of view of the detector through 360° in a plane perpendicular to the orbital plane. The radiation reflected from the scan mirror is chopped at the focus, passes through a filter, and is refocused at the lead selenide detector. The output of the detector is directly proportional to the radiation received from the earth. In-flight calibration is achieved through alternate views of space and the spacecraft housing, the temperature of which is monitored during each scan.

The effective spectral response of the radiometer is defined as

$$\Phi_\lambda = R_\lambda F_\lambda A_\lambda,$$

[1] On leave from the Faculté des Sciences, Marseille, as a National Academy of Sciences-NCR Post Doctoral Associate.
Present address: University of Delaware, College of Marine Studies, Newark, Delaware, U.S.A.

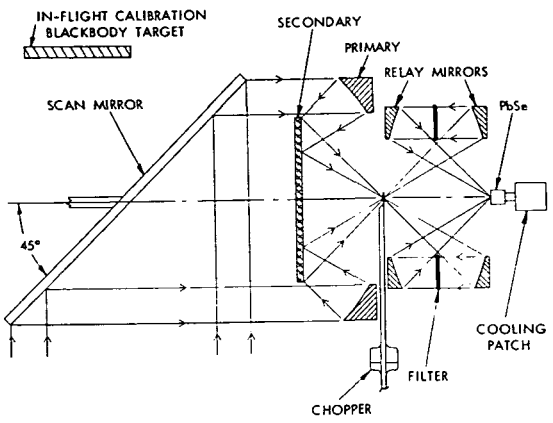

Figure 1. The principle of the measurements to detect earth radiation with a scanning radiometer in orbit.

where R_λ gives the combined spectral reflectivity of all front surface mirrors, F_λ is the spectral transmittance of the filter, and A_λ is the spectral response of the detector.

Preflight calibrations were made in the laboratory, with the radiometer's field of view being filled with a blackbody target whose temperature could be varied. The spectral radiance of the target with equivalent blackbody temperature (T_{BB}) is determined by the Planck function, B_λ.

The effective radiance $\bar{N}$ received at the radiometer is given in the following equation:

$$\bar{N} = \int_0^\infty B_\lambda(T_{BB})\varphi_\lambda d\lambda.$$

The effective radiance N for the orbiting radiometer is the λ-integral of the spectral radiance N_λ in the direction of the satellite from the earth and its atmosphere multiplied by the spectral response φ_λ:

$$\bar{N} = \int_0^\infty N_\lambda \varphi_\lambda d.$$

All measurements from orbit must be expressed in terms of the equivalent temperature of a blackbody (T_{BB}) filling the field of view of the radiometer that would cause the same response at the radiometer.

Data processing

The analog signals obtained from the HRIR aboard the satellite were digitized and computer processed; calibration and the geographic coordinates were applied automatically on the digital tape. This NMRT-HRIR (Nimbus Meteorological Radiation Tape) was used to generate grid print maps. For the study along the Somali Coast, Mercator projection charts

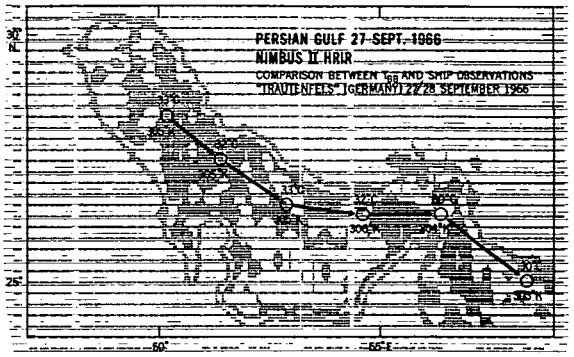

Figure 2. Comparison between ship observations and satellite infrared recordings. The coastline is produced from a contouring programme.

of 1:2 000 000 scale have been printed by computer; only in a few cases, where more detailed information was required, were charts in the 1:1 000 000 Mercator format used. A mathematical filter to eliminate a 200 Hz component in the noise level was developed by McMillin (1969) and applied in the following study. All data recorded from the orbiting radiometer within a nadir angle greater than 60° were eliminated during the computer processing of the charts.

The selected orbits showed the region of study in the centre of the satellite track; a nadir angle of less than 40° can be assumed for the reported results. Thus, the absorption of radiation by atmospheric gases could be assumed constant over the whole angle of view. An error less than 1 C° is produced by this assumption (Kunde, 1965). To reduce the error of geographic referencing from the computer, thermal gradients between water and land masses were used to indicate more accurate coastlines. An example is seen in Figure 2, where the coastline from the Persian Gulf can be reproduced from the sharp thermal gradient recorded with the Nimbus infrared radiometer. Comparison between the coastlines indicated on the working and nautical charts showed a deviation of the order of 0·5°. This small deviation was found also near the Somali Coast, where, in general, the computer-produced geographic reference error was less than 0·2°. For the entire study, the orbits with a visible error in the pitch axis were already omitted.

Results

Test area Persian Gulf

The Persian Gulf has been chosen as a test area over which to investigate the ground truth (validity as established by ground data) for the two following studies:

1) The relative accuracy of the recorded T_{BB} values aboard the satellite. The second study has been made with reported ship temperatures in the Persian Gulf.
2) The seasonal fluctuation of temperatures recorded by a satellite in a given region.

Hydrographic features in the Persian Gulf

The Persian Gulf resembles a Mediterranean Sea with an arid climate; that is, evaporation exceeds precipitation, and water is formed with a high salinity. This increase in salinity takes place during the transport of surface water from the Gulf of Oman through the Strait of Hormuz to the northern edge of the Persian Gulf, as a result of the excess of evaporation over precipitation. Consequently, water with density as high as $\sigma_t = 26$ is formed at the surface and will sink to the bottom. This dense, warm, and saline water will then be transported over the bottom into the neighbouring Arabian Sea.

The formation of highly saline water is not limited to the summer months; it is a continuous process and depends on winds and temperature. The supply of river water from the Euphrates and Tigris is limited to a small region of the gulf and can be traced by low salinities, lower temperatures, and lower densities southward along the Arabian Coast. A freshening of the northern gulf water by the greatest runoff from the Euphrates and Tigris occurs during spring and early summer; this results from snow melting in the Armenian mountains (Table 1).

A yearly fluctuation in temperature is evident: a mean temperature of 15°C was observed during February in the northwest corner of the Persian Gulf; the maximum reported up to now is 36°C for the southern Persian Gulf, as shown in Table 2.

At the end of the Southwest Monsoon, a heating of the upper water layer is introduced, and temperature values of up to 33°C were observed by Emery (1956); also, 36·5°C has been reported by Blegvad (1944) near the Bahrein Islands. The big change of temperatures from about 36°C in summer to about 15°C in February was reported at Bandare Shahpur.

Table 1. Mean salinities (S ‰) in the Persian Gulf as averaged from data reported by Dubach (1964).

Month	Location (East Longitude)						
	48°–49°	49°–50°	50°–51°	51°–52°	52°–53°	53°–54°	54°–56°
May	–	39·92	39·73	38·85	38·85	–	37·97
Jun	26·09	39·93	–	38·94	37·75	37·84	37·46
Jul	–	–	–	–	–	–	–
Aug	–	–	39·39	39·50	38·68	39·54	38·79
Sept	–	–	–	–	–	–	–
Oct	–	40·27	39·67	39·44	38·00	39·54	38·12
Nov	40·70	40·26	40·01	–	–	–	–
Dec	40·06	–	40·02	–	–	–	–

Table 2. Mean temperatures (°C) in the Persian Gulf, after Schott (1908).

Month	Location (East Longitude)						
	48°–49°	49°–50°	50°–51°	51°–52°	52°–53°	53°–54°	54°–55°
Dec	18·4°	20·3°	21·6	22·6	23·3	23·5	24·2
Jan	16·0°	17·3°	19·7	20·8	21·1	21·4	22·1
Feb	15·2°	16·4°	18·1	19·4	19·8	20·9	21·8
Mar	17·0°	17·7°	19·1	20·0	20·8	21·8	22·0
Apr	19·8°	20·7°	22·0	22·6	23·2	23·8	24·1
May	24·5°	25·0°	25·5	26·0	26·3	26·9	27·0
Jun	27·4°	27·8°	28·4	28·2	28·4	28·6	28·9
Jul	29·6°	29·8°	30·4	30·4	31·2	31·0	31·0
Aug	31·9°	31·5°	31·2	31·8	32·0	32·4	32·3
Sep	29·8°	30·6°	31·1	31·7	31·8	31·9	31·8
Oct	27·5°	28·7°	29·4	29·6	29·9	30·3	30·5
Nov	22·8°	24·1°	25·6	26·1	27·3	27·6	27·9
No. of observations	86	243	595	326	260	241	242
Yearly average	23·3°C	24·2°C	25·2°C	25·8°C	26·2°C	26·7°C	27·0°C
Absolute maximum	33·1°C	33·1°C	34·5°f	34·2°C	34·5°C	36·0°C	34·9°C
Date	11 Aug	21 Aug	5 Aug	17 Aug	17 Aug	17 Aug	21 Aug
Absolute minimum	13·8°C	12·3°C	15·8°C	16·3°C	18·0°C	17·9°C	17·9°C
Date	20 Feb	22 Jan	20 Feb	20 Feb	10 Mar	12 Feb	17 Jan

Table 3. Comparison of sea surface temperatures observed by ships and Nimbus 2 in the Persian Gulf during 1966

Date	GCT	Latitude (°N)	Longitude (°E)	Clouds	Sea temperature measured from ship (°C)	Δt (air–sea, in C°)	T_{BB} (°C)	Δt (T_{BB}–t, in C°)	Ship
3 Jun.....	12/18	24°30′	58°30′	0	32(2)	−1	31	−1	Kenai Peninsula
8 Jun.....	12/18	24°30′	59°00′	0	29(2)	+3	33	+4	Torrey Canyon
13 Jun.....	00/06	24°30′	58°00′	0	32(2)	±0	33	+1	Mobil Brilliant
16 Jun.....	06	27°00′	53°00′	0	29	+2	30	+1	Esso Chile
	12	26°00′	54°00′	0	32	−1	31	−1	
	18	26°00′	56°00′	0	32	−2	31	−1	
17 Jun.....	00	26°00′	57°00′	0	32	−1	33	+1	Esso Chile
	06	25°00′	58°00′	3	32	−1	33	+1	
	12			0	32	+1	31	−1	
5 Jul.....	06	26°00′	54°00′	0	32	±0	31	−1	Northfield
4 Sep.....	00	28°00′	51°00′	0	34	−2	32	−2	Petroqueen
	06	27°00′	52°00′	0	34	±0	34	±0	
	12	26°00′	54°00′	0	35	−2	33	−2	
17 Sep.....	12	26°00′	55°00′	0	33	+1	32	−1	Petroqueen
	18	26°00′	53°00′	0	34	−2	32	−2	
23 Sep.....	06	29°00′	50°30′	0	33	±0	33	±0	Trautenfels
27 Sep.....	00	28°30′	50°00′	0	33	−2	32	−1	Trautenfels
	06	27°30′	51°30′	0	32	−4	33	+1	(see Fig. 8)
	12	26°30′	53°00′	0	33	−1	33	±0	
	18	26°30′	54°30′	0	32	−1	33	+1	
28 Sep.....	00	26°30′	56°00′	1	30	−1	30	±0	
	12	25°00′	59°30′	1	30	−1	30	±0	
3 Oct.....	18	24°30′	58°00′	8[1]	29	±0	28	−1	Wabasha
3 Oct.....	12	24°30′	58°00′	0	30	+6	31	+1	Petersen
	18	26°00′	57°00′	0	30	−1	30	±0	
4 Oct.....	00	26°30′	55°30′	0	32	−2	31	−1	Petersen
	06	27°00′	54°00′	0	33	+1	33	±0	

[1] Uncertain.

Statistical comparison between ship observations and satellite SST measurements

The statistical treatment of the difference between T_{BB} values and temperatures reported from ships is based on 27 observations. The T_{BB} resulting from a 1:2 000 000 grid print map were compared with reports from ships, whose positions were determined within the corrected grid print map position as described above. The results are given in Table 3.

The mean value showed that the satellite radiation temperature was 0·1°C below that indicated by ship data. The calculated standard deviation for the *difference* between ship data and T_{BB} values was 1·3°C. However, the diurnal cycle of the surface temperatures in the Persian Gulf is included in the above calculation, because only in a few cases were temperature measurements aboard ships made during satellite overpass. Also, errors in ship measurements must be taken into account. That suggests that the absolute error will be less than calculated from the ship and satellite observations.

A comparison between actual T_{BB} values and ship observations is seen in Figure 2, where six ship temperature values were available over 24 h and are included in the grid print HRIR map for 27 September.

Seasonal temperature changes observed with the HRIR

For the purpose of this Nimbus 2 HRIR study, all available cloud-free orbits made during the night over the Persian Gulf from June through September 1966 were analyzed from computer-produced grid print maps.

Mean T_{BB} values were calculated for the Persian Gulf from approximately 350 scan spots that covered individual areas 9 to 12 km in diameter for the northern and southern regions. The regions covered are shown by the two squares in Figure 3.

Historical sea surface temperatures (SST's) for these two regions indicated a seasonal SST range of 15°C and a 1·7°C regional temperature difference between the southern and northern areas. The satellite indicated two pronounced temperature markings: one in mid-June and the other in mid-September 1966 (Warnecke et al, 1971).

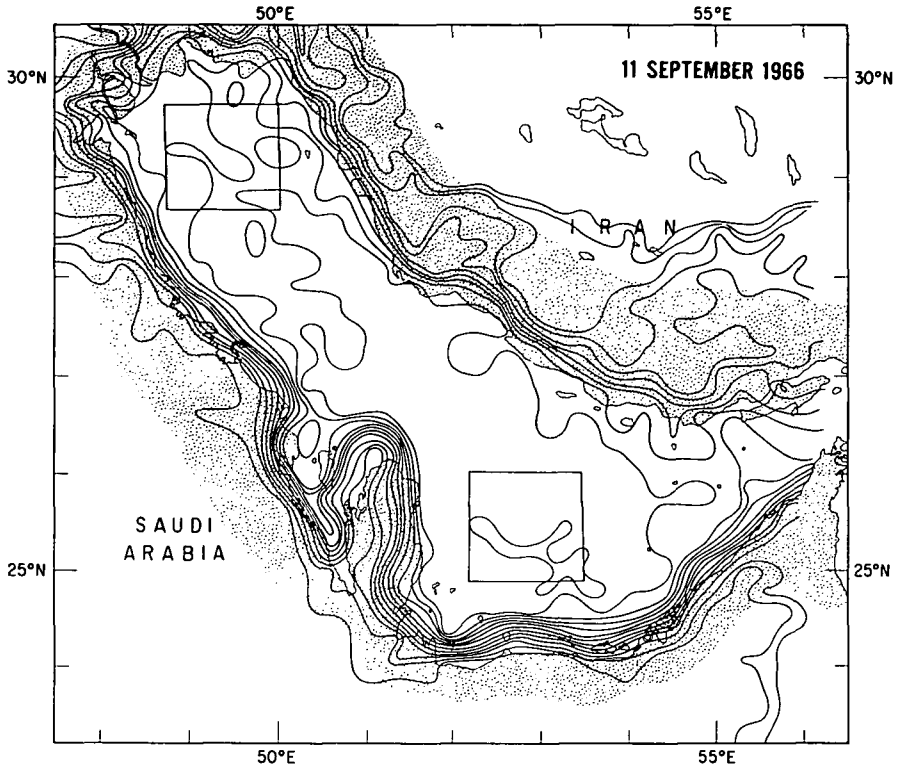

Figure 3. Gradients obtained from Nimbus HRIR over the Persian Gulf on 11 September 1966. Included in this analysis is the coastline obtained from a nautical chart.

In mid-June, extremely high air temperatures between 49°C and 46°C were recorded by weather stations in the area, (Szekielda, Salomonson and Allison, 1972). The Persian Gulf sea surface temperature changes follow the changes in surface air temperature; we might expect high SST's from high air temperatures alone.

A mean difference of 1·3°C was noted between averaged night-time HRIR data over the warmer southern portion of the gulf and corresponding data over the cooler northern portions;this agrees with historical SST data of 1·7°C mean difference.

An example of the cold water in the northern Persian Gulf is shown in Figure 4. Cold water can be recognized by the position of the 29°C isotherm and the well-developed gradient. Figure 5 shows the position of the warm water in the southern part of the Gulf.

Test area Somali Coast

In connection with the upwelling along the Somali Coast strong horizontal temperature gradients appear (Düing and Szekielda, 1971; Szekielda, 1972). This area was selected to test the feasibility of monitoring temperature gradients and temperature patchiness from an orbiting platform.

During the South-west Monsoon, the Somali Current flows in a northerly direction as a western boundary current from below the equator. Contrary to the other western boundary currents (e.g., the Kuroshio and the Gulf Stream), the Somali Current sets at about 9°N in an eastern direction and then turns into an anticyclonic surface current at a distance of about 150 n. miles from the coast. Investigations in August and September of 1964 revealed that the Somali Current is a very well defined and intense narrow stream (Strommel and Wooster, 1965). It differs only in a few points from the other currents mentioned. The most important point is that the Somali Current is present for only part of the year. Just north of the region where the current leaves the coast, strong upwelling appears; temperatures as low as 13°C appear. The intensity of the upwelling along the Somali Coast depends upon the geostrophic slope of the isotherms, which are a function of the strength of the current. Therefore, upwelling along the Somali Coast depends upon the wind stress and the monsoon season.

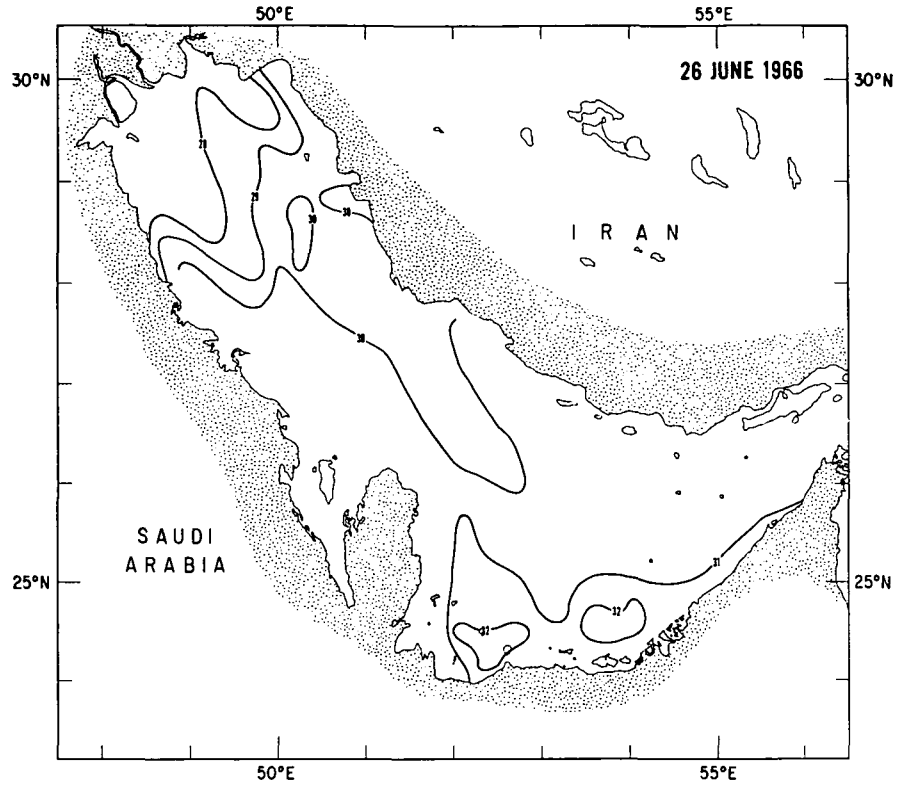

Figure 4. Temperature distribution, in °C, in the Persian Gulf on 26 June, 1966.

Temperature patchiness and temperature gradients

For a comparison with the temperature patchiness as recorded by the satellite HRIR, only a few ship measurements along the Somali Coast were available. Szekielda (1971) reported a comparison between ship reports and satellite measurements for this area.

Observations from orbits on 13 and 16 August showed (Figure 6) that the greatest temperature gradients are limited to the region near the coast and in the water between the Gulf of Aden and the adjacent sea. No ship data were available for 13 and 16 August, but one ship crossed the upwelling area during 21 and 22 August (Table 4). Although the centre of the upwelling water was not crossed, a minimum temperature of 23·3°C was recorded. The temperature change of 6°C between 10°54′N 52°06′E and 12°0′N 49°24′E marked the sharp temperature gradient at the exit of the Gulf of Aden.

Table 4. Sea surface temperatures observed aboard the SS "Steel Fabrication" during 21 and 22 August 1966.

Date	Position		SST
	Latitude N (degrees)	Longitude E (degrees)	(°C)
21 August ..	8°48′	54°12′	26·1
	9°36′	53°18′	25·6
	9°42′	52°42′	24·4
	10°54′	52°06′	23·3
22 August...	12°00′	49°24′	29·4
	11°54′	47°54′	31·1
	11°48′	46°18′	30·6

Figure 7 shows an unusual temperature gradient found at the eastern border of the Gulf of Aden on 4 September (see also Szekielda and Mitchell, 1972). Ship observations confirmed the presence and the strength of this gradient and its variation with time and latitude. Observations from the ships that crossed the Gulf of Aden are shown in Figure 8. The greatest temperature change was reported by the "Forsvik" during 20 and 21 September when it crossed the gulf off its southern coast. The "President Jackson" crossed the gulf a few weeks earlier off the northern edge and reported only a small temperature gradient, although a temperature decrease of 5°C over 360 n. miles was observed from west to east. On the other hand, the "Universe Defiance" had recorded a

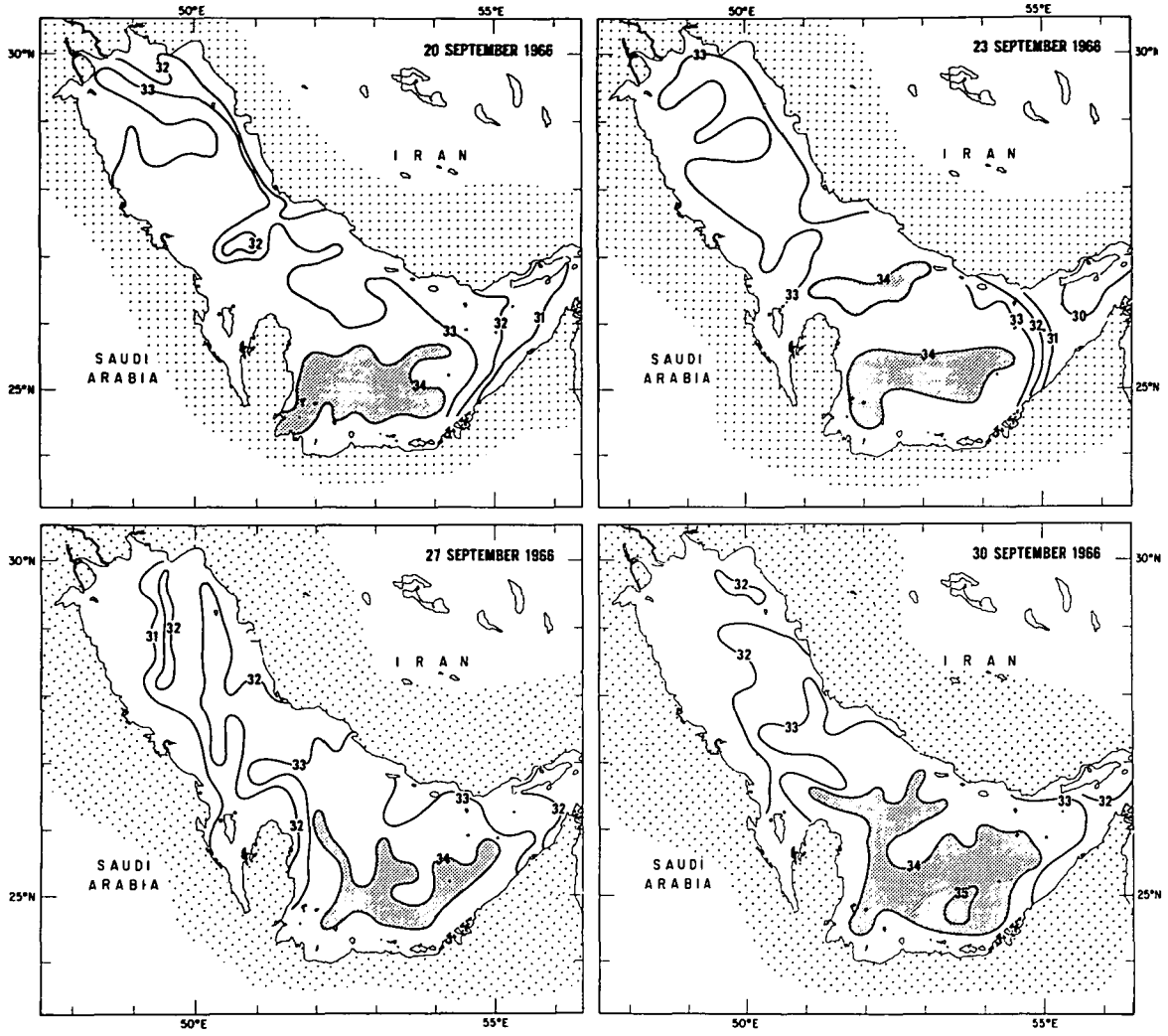

Figure 5. Observations over the Persian Gulf. Shaded areas show water temperatures above 34°C.

sharp temperature gradient at 13°N. These results coincide with the satellite measurements.

Conclusion

The comparisons between ship data and infrared recordings from satellites show that reliably accurate measurement of sea surface temperatures can be obtained from satellite altitudes. The results presented in this paper were obtained from an area with an arid climate and only cloud free areas were analyzed. With the help of the infrared pictorial display a decision was made regarding whether or not the field of view of the radiometer was cloud contaminated. No information about the vertical distribution of water vapour was included. Therefore the temperature pattern and temperature gradients have to be considered as relative values. However, future sensors, monitoring the oceans outgoing radiation at different wavelength, could help to receive absolute temperatures from a platform in orbit.

Acknowledgments

The author wishes to thank Dr. W. Nordberg, chief of the Laboratory of Earth and Meterological

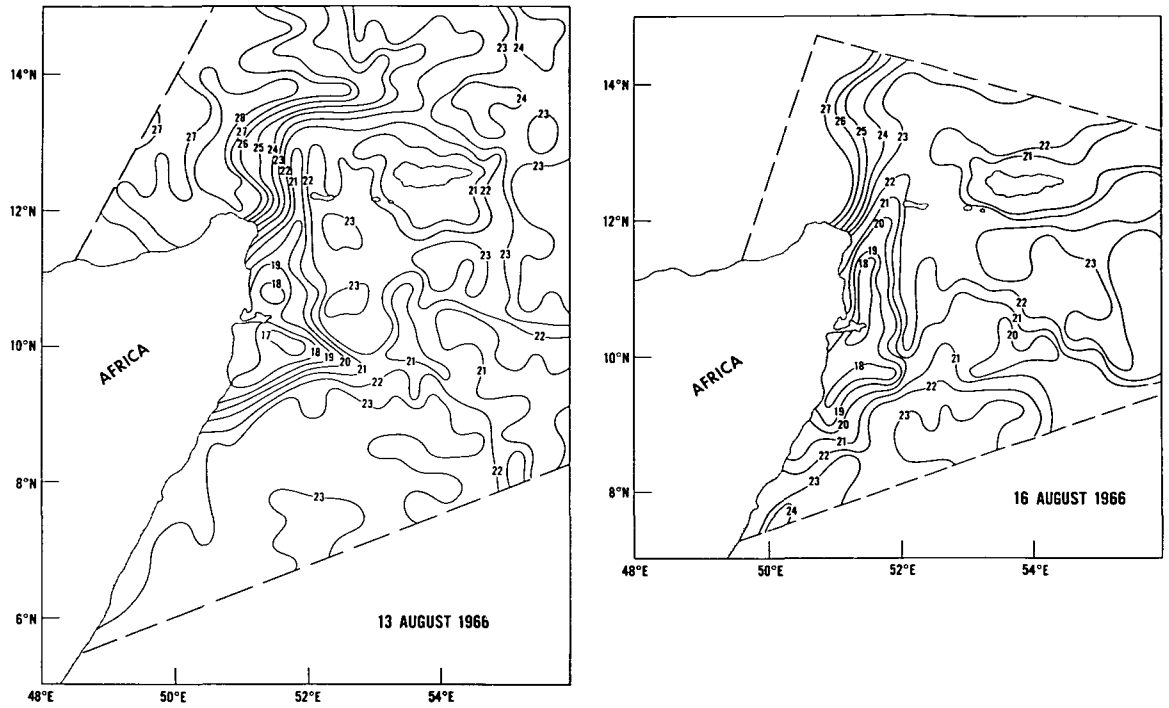

Figure 6. T_{BB} distribution along the Somali Coast.

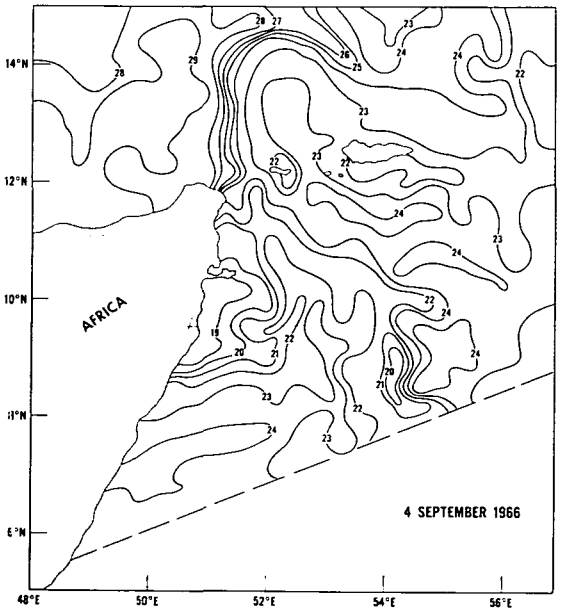

Figure 7. T_{BB} distribution along the Somali Coast.

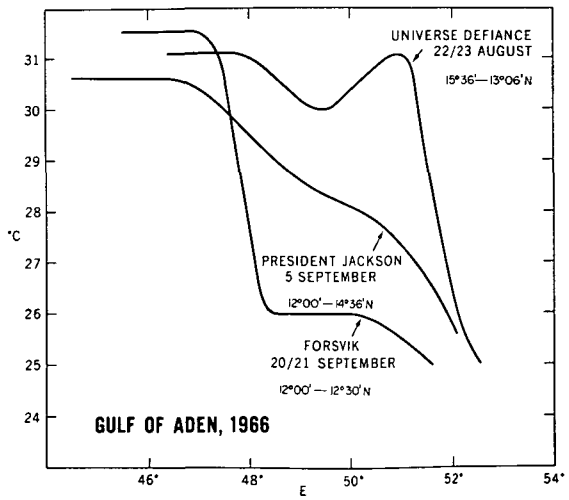

Figure 8. Temperature distribution in the Gulf of Aden.

Sciences, and W. R. Bandeen, assistant chief, for the use of the excellent working facilities in their laboratory. Miss J. E. Regalla gave important help in computer processing the HRIR data.

References

Blegvad, H. 1944. Fishes of the Iranian Gulf. *In* Danish scientific investigations in Iran. (3) 247 pp. Ed. by K. Jessen and R. Spärck. Munksgaard, Copenhagen.

Dubach, H. W. 1964. A summary of temperature-salinity characteristics of the Persian Gulf. Nat. Oceanogr. data center (G4), U.S. Naval Oceanographic Office, Wash. 223 pp.

Düing, W. & Szekielda, K.-H. 1971. Monsoonal response in the Western Indian Ocean. J. geophys. Res. 76: 4181–7.

Emery, K. O. 1956. Sediments and water of the Persian Gulf. Bull. Am. Ass. Petrol. Geol. 40: 2354–83.

Kunde, V. 1965. Theoretical relationship between equivalent blackbody temperature and surface temperatures measured by the Nimbus high resolution infrared radiometer. *In* Observations from the Nimbus I Meteorological Satellite. NASA Spec. Publ. (89) 117 pp.

LaViolette, P. E. & Seim, S. E. 1969. Satellites capable of oceanographic data acquisition – a review. Tech. Rep. hydrogr. Off. Wash. 215: 81 pp.

McMillin, L. M. 1969. A procedure to eliminate periodic noise found in Nimbus II high resolution infrared radiometer measurements. NASA Contract. Rep. 9 G45–32: 16 pp.

Pouquet, J. 1968. An approach to the remote detection of earth resources in subarid lands. NASA Tech. Note D4647: 87 pp.

Schott, G. 1908. Der Salzgehalt des Persischen Golfes und der angrenzenden Gewässer. Annln Hydrogr. Berl. 36: 296–9.

Stommel, H. & Wooster, W. 1965. Reconnaissance of the Somali Current during the Southwest Monsoon. Proc. nat. Acad. Sci. Wash. 54: 8–13.

Szekielda, K.-H. 1971. Anticyclonic and cyclonic eddies near the Somali Coast. Dt. hydrogr. Z. 24: 26–9.

Szekielda, K.-H. & Mitchell, W. 1972. Oceanographic applications of color-enhanced satellite imageries. Remote Sensing of Environment, 2: 71–6.

Szekielda, K.-H., Salomonsen, V. V. & Allison, L. J. Seasonal sea surface temperature variations in the Persian Gulf as recorded by Nimbus 2 HRIR (in press).

Szekielda, K.-H. 1972. Upwelling studies with satellites. J. Cons. int. Explor. Mer 34: 379-88.

Warnecke, G. Allison, L. J., McMillin, L. M. & Szekielda, K.-H. 1971. Remote sensing of ocean currents and sea surface temperature changes derived from the Nimbus II satellite. J. phys. Oceanogr. 1: 45–60.